

Article

Volume Stability and Mechanical Properties of Cement Paste Containing Natural Fibers from Phragmites-Australis Plant at Elevated Temperature

Hassan Ghanem ^{1,*} , Rawan Ramadan ¹, Jamal Khatib ¹  and Adel Elkordi ^{1,2} 

¹ Faculty of Engineering, Beirut Arab University, Beirut 12-5020, Lebanon; r.ramadan@bau.edu.lb (R.R.); j.khatib@bau.edu.lb (J.K.); a.elkordi@bau.edu.lb (A.E.)

² Department of Civil and Environmental Engineering, Faculty of Engineering, Alexandria University, Alexandria 5424041, Egypt

* Correspondence: h.ghanem@bau.edu.lb

Abstract: The utilization of bio-fiber materials in building components has become imperative for improving sustainability, controlling global warming, addressing environmental concerns, and enhancing concrete properties. This study is part of a wide-range investigation on the use of Phragmites-Australis (PhA) fibers in construction and building materials. In this paper, the volume stability and mechanical properties of paste containing PhA fibers and exposed to high temperatures were investigated. Four mixes were made with 0, 0.5, 1, and 2% fibers by volume. To evaluate the volume stability and mechanical properties, the chemical shrinkage, autogenous shrinkage, drying shrinkage, expansion, ultrasonic pulse velocity, compressive strength, and flexural strength were tested. The curing duration and temperature were 180 days and 45 °C, respectively. The results indicated that an addition of PhA fibers of up to 2% resulted in a reduction in all the shrinkage parameters at 180 days. The presence of PhA fibers in the paste tended to reduce the compressive strength, with the lowest value observed at 2%. Apart from the values at 90 days, the optimal flexural strength seemed to be achieved by the paste with 1% PhA fibers. To further elucidate the experimental results, a hyperbolic model was employed to predict the variation in the length change as a function of the curing age with a high accuracy. Based on the results obtained, PhA fibers can play a crucial role in mitigating the shrinkage parameters and enhancing the mechanical properties of cement paste.

Keywords: bio-fiber; volume stability; mechanical properties; cement paste; elevated temperature



Citation: Ghanem, H.; Ramadan, R.; Khatib, J.; Elkordi, A. Volume Stability and Mechanical Properties of Cement Paste Containing Natural Fibers from Phragmites-Australis Plant at Elevated Temperature. *Buildings* **2024**, *14*, 1170. <https://doi.org/10.3390/buildings14041170>

Academic Editor: Chenggao Li

Received: 15 March 2024

Revised: 12 April 2024

Accepted: 16 April 2024

Published: 21 April 2024



Copyright: © 2024 by the authors. Licensee MDPI, Basel, Switzerland. This article is an open access article distributed under the terms and conditions of the Creative Commons Attribution (CC BY) license (<https://creativecommons.org/licenses/by/4.0/>).

1. Introduction

Achieving a sustainable concrete structure involves minimizing the total societal impact during the structure's entire life cycle, which includes short-term consequences (immediate environmental disruption, increased energy consumption during construction, and potential social dislocation due to construction activities) [1–3] as well as long-term consequences (carbon emissions associated with material production, the degradation of ecosystems, infrastructure maintenance costs, and resilience to environmental change effects) [4,5]. The creation of durable structures is important for decreasing their long-term impact. Sustainable construction can reduce the project and operating costs of buildings and infrastructure. The use of supplementary cementing materials (SCMs) [6–10] and chemical admixtures and the evaluation of the impact of building materials on local and worldwide air conditions are critical for constructing cost-efficient, environmentally friendly, and durable structures [11,12].

A wide range of fibers, including steel, synthetic, and natural fibers, have been used to reinforce composites such as cement paste, mortar, and concrete to improve properties such as the tensile strength, shear strength, and durability. Natural fibers of a vegetable origin, such as coconut husk, sisal, sugarcane bagasse, jute, bamboo, and wood fibers, have

recently gained interest for use in low-cost housing construction due to their commercial prospects and potential to reduce the foreign reserve expenditure on imported fibers. For example, the addition of sisal fibers to concrete results in improved compressive and flexural strength, as well as reduced drying shrinkage [13]. A study found that the addition of coconut fibers to concrete resulted in improved tensile strength and toughness [14]. Also, the use of natural fibers such as jute or coir in concrete has been found to improve the concrete's resistance to cracking and impact strength [15]. A study investigating the use of date palm fibers in concrete indicated that palm fibers improve the flexural and compressive strength, as well as reduce the permeability and chloride ion penetration [16].

In addition to that, natural fibers can be added to a concrete mix as a way to control elevated concrete temperatures. These fibers can act as insulation, reducing the heat generated by the cement hydration process and slowing down the rate of temperature rise. According to some studies, the use of natural fibers such as rice husk ash, coconut fibers, and palm fibers can help to reduce the temperature of concrete. For example, a study showed that concrete with the addition of kenaf fibers exhibited the lowest tensile strength and Young's modulus (E) at 100 °C, with the highest values observed at 20 °C [17]. Another investigation focused on the influence of temperature (180–220 °C) on various natural fibers over predetermined durations (5, 10, 15, 30, 60, and 120 min). The findings showed that degradation occurred more rapidly at higher temperatures [18]. Furthermore, a study highlighted the use of lignocellulosic fiber degradation around 200 °C. The results emphasized the susceptibility of natural fibers to elevated temperatures in cementitious composites, likely due to their poor thermal conductivity compared to the concrete matrix [19,20]. In addition, changes in the strain along the length of the jute fibers and within the cement matrix with increasing temperatures have been documented. These alterations caused the jute fibers to contract (around 5.8% at 200 °C) as the water held by them was released, leading to the collapse of the cell walls [21].

It is important to mention that the use of *Phragmites-Australis* (PhA) fibers in concrete is still a relatively new and unexplored field. PhA is a highly versatile plant and has been used for various purposes throughout history, such as for thatching roofs, for making paper and musical instruments, and as forage for livestock. Lately, this plant has found several applications in construction materials, particularly in the utilization of its stems [22]. PhA, commonly known as the common reed, is found on every continent except Antarctica. It can grow with a maximum height of 4.6 m [23]; the characteristics of the PhA plant, including its stems and leaves, are detailed in Figure 1. In Lebanon, it particularly flourishes in substantial quantities in the eastern part of the Bekaa Valley, where its rapid growth causes problems for local farmers in terms of disposal. The conventional method of burning the plant, employed to tackle this issue, raises concerns about its potential environmental impact, contributing to pollution. Consequently, recent studies have been directed towards investigating sustainable solutions, exploring the incorporation of such plant into construction materials, and assessing its potential effects in a more ecologically friendly manner. For example, a study demonstrated that incorporating 0.5% PhA fibers enhanced the load deflection of RC beams [24]. Furthermore, the results of another study revealed that the addition of PhA fibers of up to 2% resulted in a reduction in the shrinkage parameters [25].

Given the limited existing research on the utilization of PhA plants in cementitious applications, particularly under elevated temperatures, this study aimed to address this gap. This work focused on investigating how the addition of these fibers affects the mechanical properties and length stability of cement paste. The primary objective was to provide a precise understanding of the performance of PhA in cementitious materials under elevated-temperature conditions, satisfying a crucial knowledge gap in this specific application domain.

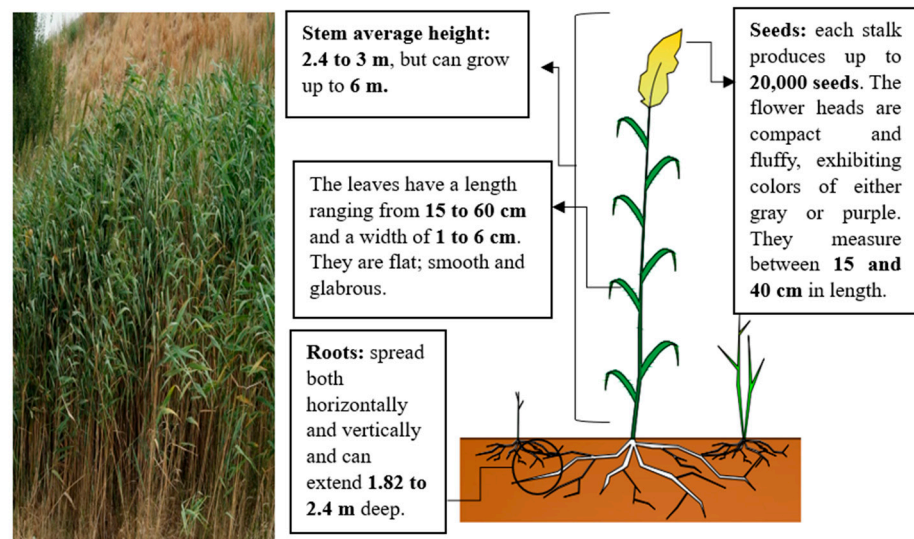


Figure 1. PhA plant dimensions.

2. Materials and Methods

2.1. Raw Materials

The production of all paste mixtures utilized a range of materials, including ordinary Portland cement (OPC), distilled water, and PhA fibers with a density of 665 kg/m^3 . The PhA fibers used in this study were 10 mm in length and were added to the mixtures in proportions of 0.5%, 1%, or 2% by volume. The maximum addition of 2% PhA fibers was chosen based on a series of trial mixes and previous research [26,27]. Beyond the 2% level, it was found that the mechanical properties such as the compressive strength significantly dropped [28,29]. All the fibers were treated with a 4% NaOH solution for 24 h. After treatment, the fibers were washed with water, dried, and stacked in bags. The procedure for obtaining PhA fibers is illustrated in Figure 2.

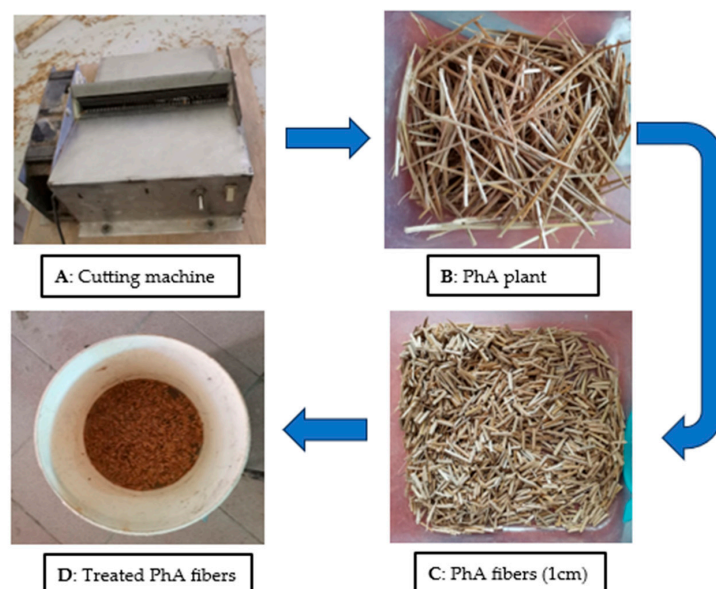


Figure 2. Process of preparing the PhA fibers.

2.2. Paste Specimen Preparation

After conducting several trials, this study employed a paste with a water-to-cement (W/C) ratio of 0.55. Four cement paste mixes were prepared, as presented in Table 1.

Initially, the dry constituents, cement and PhA fibers, were dry-mixed for 1 min, and then the required amount of water was added. The constituents were then mixed for 3–5 min until a homogenous mix and a uniform dispersion of fibers was achieved, taking care not to overmix and cause damage or a loss of strength to the fibers. In addition, the molds were thoroughly oiled before casting to ensure a fair face casting and facilitate remolding. After casting, the specimens were covered with nylon sheets to prevent evaporation and stored in an oven at a temperature of 45 ± 1 °C. After 24 h, the specimens were demolded and soaked in water at a relatively constant oven temperature of 45 ± 1 °C until testing.

Table 1. Mix proportions.

Paste Code	Quantity (kg/m ³)			W/C *
	Cement (C)	Water (W)	PhA Fibers	
P0%PhA	1152.8	634.04	0	0.55
P0.5%PhA	1152.8	634.04	3.33	0.55
P1%PhA	1152.8	634.04	6.65	0.55
P2%PhA	1152.8	634.04	13.3	0.55

* Water-to-cement ratio.

2.3. Testing Procedure

Several tests were conducted to determine the volume stability and mechanical properties of the pastes. The tests conducted for volume stability were chemical shrinkage (CH-S), drying shrinkage (DR-S), autogenous shrinkage (AU-S), strength, and expansion (EXP) tests. To measure the shrinkage of the paste samples, steel molds with dimensions of 25 mm × 25 mm × 285 mm were used to cast the samples. After 24 h, the samples were removed from the molds and prepared for shrinkage measurements. Two demec points were applied to two sides of the samples at 200 mm. The DR-S, AU-S, and EXP were measured by testing the samples according to ASTM C490 [30]. For DR-S, the samples were placed in the oven at a constant temperature of 45 °C. For AU-S, the specimens were placed in plastic bags and sealed to prevent moisture loss, while for EXP, the samples were placed in water at a constant oven temperature of 45 °C. The length of the specimens was recorded every 2 up to 180 days (d), with three values taken per side for each sample. The average length change was taken from two specimens for each mix. The procedure for measuring the CH-S of the pastes was conducted in accordance with ASTM C1608 [31]. A freshly mixed paste (a combination of cement, PhA fibers, and water) was placed in a 250 mL glass bottle, with a thickness measuring approximately 2 cm. A 2 mL graduated pipette was then inserted through a hole in a rubber stopper and filled with water. A drop of oil was added to prevent water evaporation. Figure 3 illustrates the setup for the CH-S test.

The initial measurement was taken after one hour, with the measurements being conducted for 180 d. The CH-S is expressed as the volume reduction in the paste per gram of binder, and two replicate samples were tested for each mixture. The volume change (mL/g of binder) was converted to a length change (μm/m) using Equation (1), to allow for a comparison with the other shrinkage measurements.

$$\frac{\Delta L}{L} = \frac{\Delta V}{3V} \quad (1)$$

where:

ΔL = change in the length at time (t);

L = initial length of the sample;

ΔV = change in the volume in the pipette at time (t);

V = initial volume of the sample.

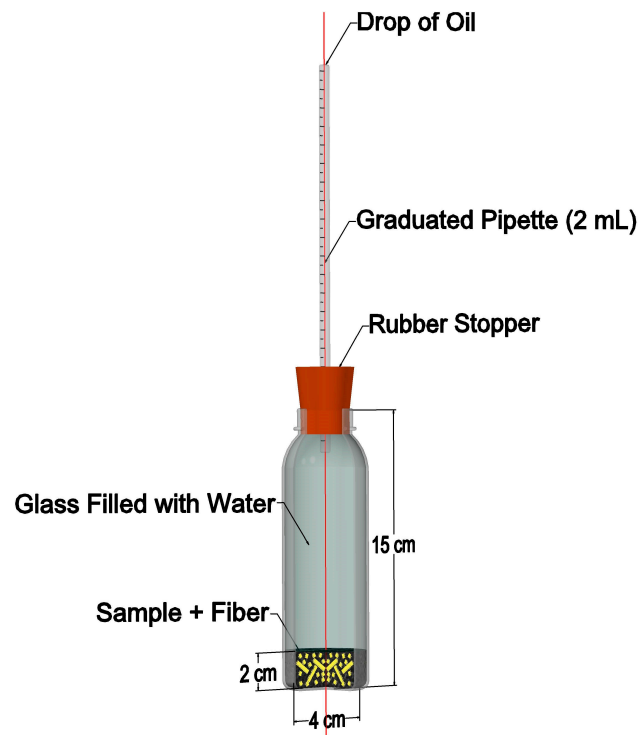


Figure 3. CH-S setup.

To test the mechanical properties of the paste samples, this research involved performing tests on the flexural strength and compressive strength using a pressing machine with a rate-loading control of 2.5 MPa/s. It should be noted that, before applying the strength test, density and ultrasonic pulse velocity (UPV) tests were performed according to ASTM C138 [32] and ASTM C597 [33], respectively. On the testing days (1, 3, 7, 28, 90, and 180), flexural strength tests were conducted on $4 \times 4 \times 16$ cm samples in a 3-axis bending scheme with the bending force applied at the center of the span between supports spaced 150 mm apart. The flexural strength was calculated as follows:

$$\sigma = \frac{3PL}{2bd^2} \quad (2)$$

where:

P = maximum load;

L = prism length;

b = prism width;

d = prism thickness.

The compressive strength test was conducted on 40×40 mm samples obtained from the flexural test in accordance with standard EN 1015-11 [34]. All the testing samples were placed in an oven at a constant temperature of 45 ± 1 °C, as shown in Figure 4.

2.4. Estimation of Length Change Parameters

Construction engineers are interested in many parameters that can characterize the volume stability of cement paste. Among those parameters are the initial rate of length change (IRLC) and the ultimate length change (ULC). The IRLC denotes the pace of shrinkage or expansion during the initial phases of volume change due to moisture loss or absorption, while the ULC indicates the maximum expected value of shrinkage or expansion after reaching a stable moisture content level. To analyze those crucial parameters

and to determine the length change (CH-S, DR-S, AU-S, and EXP) with time, a hyperbolic model (Figure 5) was used as follows [35,36]:

$$\varepsilon = \frac{t}{\frac{1}{a} + \frac{t}{b}} \quad (3)$$

where:

ε = shrinkage/expansion value ($\mu\text{m}/\text{m}$);

t = curing age;

a = IRLC values;

b = ULC values.



Figure 4. Samples for length change and mechanical property testing, placed in an oven at a constant temperature of 45 °C.

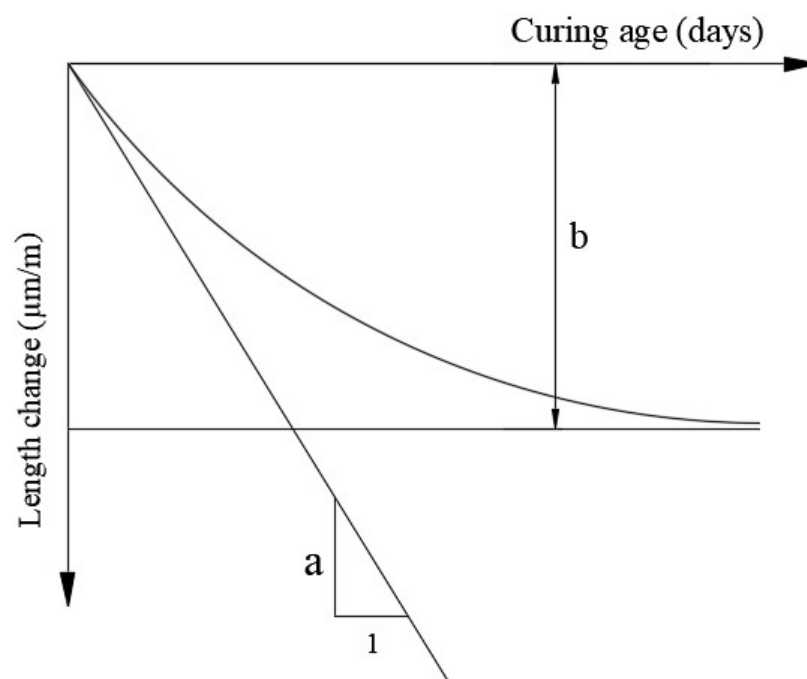


Figure 5. Initial length change rate and ultimate length change variables.

By fitting the above equation to the experimental data, the values of the IRLC and ULC were determined for each mix using the solver function in Microsoft Excel V2023.

3. Results and Discussion

3.1. Density

The densities of the pastes reinforced with varying percentages of PhA fibers are presented in Table 2. With the exception of the 1% PhA fiber mix, the inclusion of fibers resulted in a slight decrease in the density. For example, the highest density was 2250 kg/m³ for the control sample, while the lowest density of 2200 kg/m³ was recorded for the 2% PhA fiber mix at 180 days of curing. This could be partly due to the lower density of PhA fibers and the lack of proper compaction in the presence of a certain percentage of fibers, which would result in air voids in the matrix. It should be mentioned that the effects of the PhA fibers on the density depend on many parameters, such as the quantity of fibers used as well as the paste mix composition [37]. As the percentage of PhA fibers increases in the mix, the degree of compaction of the mixture decreases, which can lead to an increase in the volume of air voids within the matrix [25].

Table 2. Density of cement paste specimens at 45 °C.

Curing Age (Days)	Density (kg/m ³)			
	P0%PhA	P0.5%PhA	P1%PhA	P2%PhA
1	2060	1950	1930	2100
3	2130	2080	2150	2070
7	2160	2130	2210	2110
28	2190	2140	2223	2120
90	2210	2190	2230	2160
180	2250	2220	2240	2200

3.2. Ultrasonic Pulse Velocity (UPV)

The UPV results for the samples containing PhA fibers are depicted in Figure 6. It was evident that the inclusion of 0.5%, 1%, or 2% PhA fibers resulted in a slight reduction in the UPV at all curing ages. For example, for the control mix, the UPV at 180 d was 3.91 Km/s. This number decreased to 3.77, 3.74, and 3.71 Km/s when 0.5, 1, and 2% PhA fibers were added, respectively. This reduction in the UPV was equivalent to a 3.6%, 4.34%, and 5.10% mix, suggesting that PhA fibers have a slight impact on the cement paste matrix. This slight drop in the UPV can be attributed to several factors. First of all, the presence of PhA fibers within the paste can lead to an increase in the number of voids, consequently leading to a UPV decrease [24,25]. In addition, it can be stated that various factors, such as the type and dimensions of the fibers, the orientation and dispersion of the fibers within the material, and the specific curing conditions, can all contribute to variations in the pulse velocity [38]. Finally, the introduction of PhA fibers to the cement paste can alter the microstructure of the material by increasing the matrix porosity, which may result in a UPV reduction [39].

3.3. Compressive and Flexural Strength

The compressive strength of the pastes reinforced with varying proportions of PhA fibers is presented in Figure 7. All the mixes containing PhA fibers showed a drop in their compressive strength compared to the control mix at all curing ages. During the early age up to 3 days, it was noticed that there was little difference between all the mixes containing PhA fibers. At 3 days of curing, the drop in the compressive strength was 18, 19.2, and 26.3% compared to the reference mix. At 7 days of curing, there was a drop in the compressive strength of the mix containing 2% PhA fibers compared with the mixes containing 0.5 and 1% PhA fibers. Beyond 28 days, there was a significant drop in the

compressive strength of the 2% PhA mix compared with the other mixes. For example, the compressive strength of the control mix achieved 24.1 MPa at 180 days, whereas the mix containing 2% PhA fibers had a strength of 19.95 MPa, indicating a drop of 17.4%.

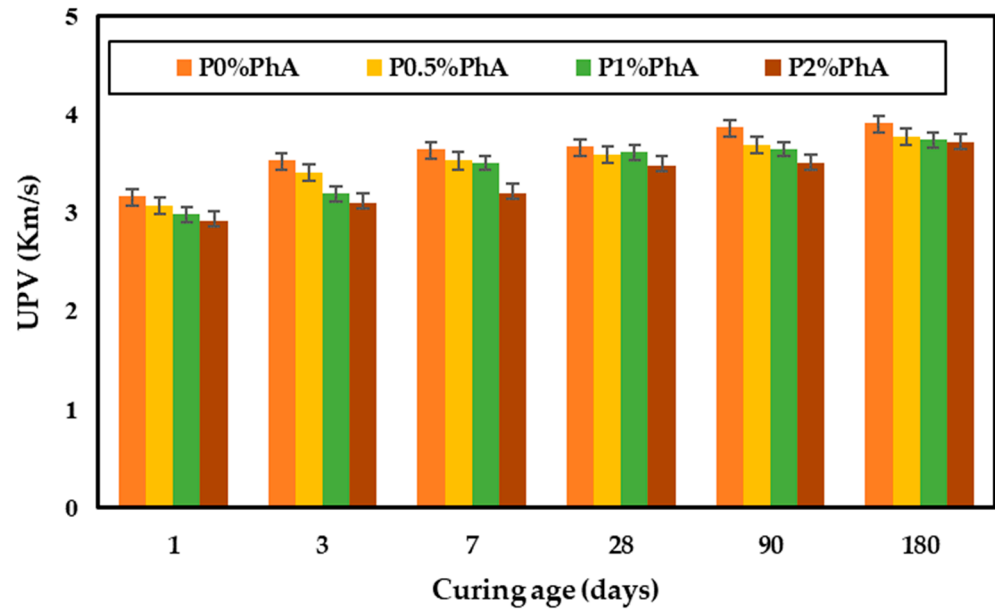


Figure 6. UPV for cement paste at 45 °C.

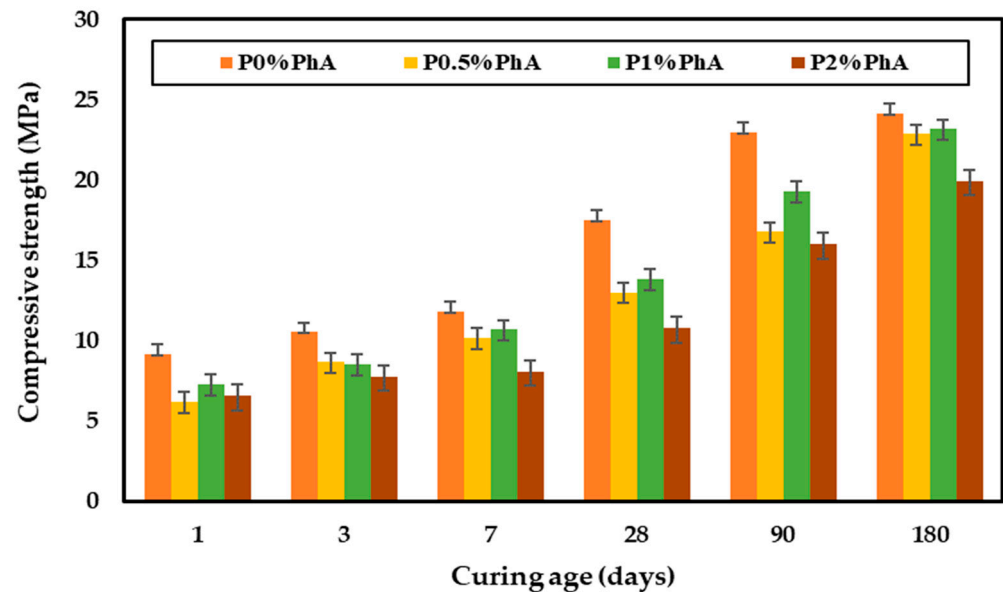


Figure 7. Compressive strength for cement pastes with different PhA fiber additions at 45 °C.

The flexural strength of the pastes with varying percentages of PhA fibers is shown in Figure 8. Apart from the values at 90 days, the optimal flexural strength seemed to be achieved by the paste with 1% PhA fibers. For example, at 180 days, the flexural strength was 9.42, 9.10, 10.19, and 7.32 MPa for the mixes containing 0, 0.5, 1, and 2% PhA fibers, respectively. This increase in the flexural strength may have been due to the strength of the fibers and the favorable physical and chemical connection between them and the paste matrix [40,41]. In addition to that, PhA fibers can restrict the propagation of microcracks, thus increasing the flexural strength of the pastes. However, the flexural strength began to decline after the addition of 1% PhA fibers due to the balling effect and improper bonding with the matrix. For example, at 180 d, the flexural strength decreased from 10.19 MPa

(1% PhA fibers) to 7.32 MPa (2% PhA fibers), which is equivalent to a 28.16% decrease. This may have been caused by the lower density of concrete at higher percentages of fiber reinforcement (2% addition) [37].

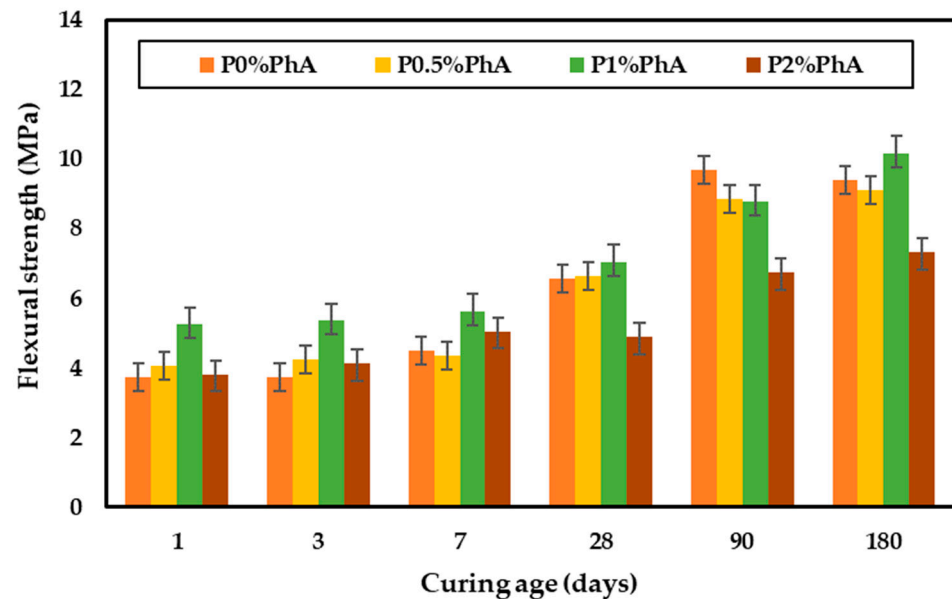


Figure 8. Flexural strength of pastes with different percentages of PhA fibers at 45 °C.

3.4. Length Change

3.4.1. Chemical Shrinkage (CH-S)

The experimental results for CH-S at an elevated temperature (45 °C) are shown in Figure 9. The CH-S for the control paste and the paste with 0.5% PhA exhibited similar values up to 180 days. However, the pastes with 1% and 2% PhA showed a decrease in CH-S compared with the control, with values of 914.4 and 840.7 $\mu\text{m}/\text{m}$, respectively. This decrease was equivalent to 8.1 and 15.3% compared to the control mix. This decrease may have been due to the presence of PhA fibers, which may have absorbed some of the heat of hydration, thereby decelerating the hydration process of the paste [35].

To further illustrate the experimental results, a hyperbolic equation to model the CH-S of the pastes yielded promising results, demonstrating a remarkable alignment with the experimental data. The coefficient of determination (R^2) was exceptionally high, with values reaching 0.984, 0.987, 0.980, and 0.981 for replacements of 0%, 0.5%, 1%, and 2% PhA fibers, respectively. This highlights the accuracy of the proposed model in describing the CH-S characteristics under elevated temperatures.

The values of the ILRC and ULC for all the paste mixes are presented in Figure 10. As shown, the ILRC did not exhibit a noticeable trend. There was a decrease for the paste with 0.5% PhA fibers, followed by an increase for 1% PhA fibers, and then a decrease again for 2% PhA fibers compared to the control. These fluctuations underscore the influence of PhA fibers on the ILRC. This effect may be attributed to the elevated temperature, which impacts the hydration process of cement [42,43]. However, there seems to be a trend in the ULC as a function of the fiber content. As the fiber content increases, the ULC decreases. For example, the ULC for the control mix was recorded at 1041.8 $\mu\text{m}/\text{m}$. This value decreased to 1006.2, 878.5, and 823.9 $\mu\text{m}/\text{m}$ for the addition of 0.5, 1, and 2% PhA fibers. This reduction was equal to a 3.4, 15.6, and 21% decrease compared to the reference mix. This decrease may have been due to the presence of PhA fibers altering the microstructure, thereby affecting the hydration mechanisms [43].

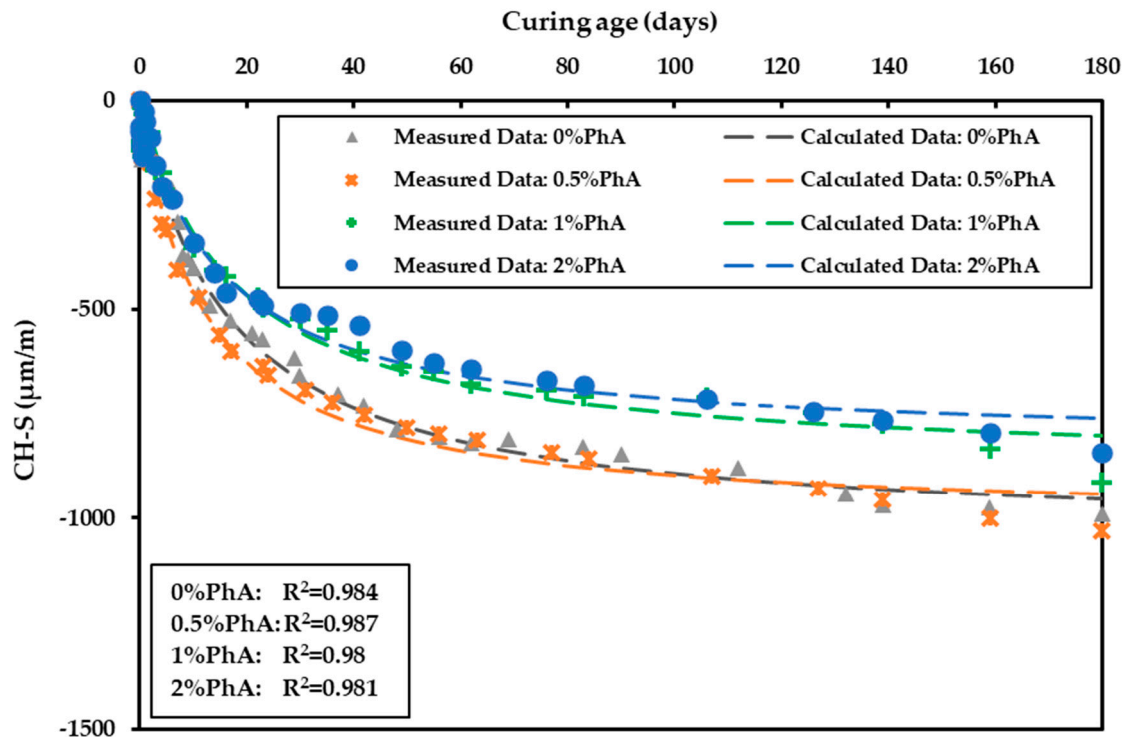


Figure 9. Estimation of CH-S for cement paste samples at 45 °C.

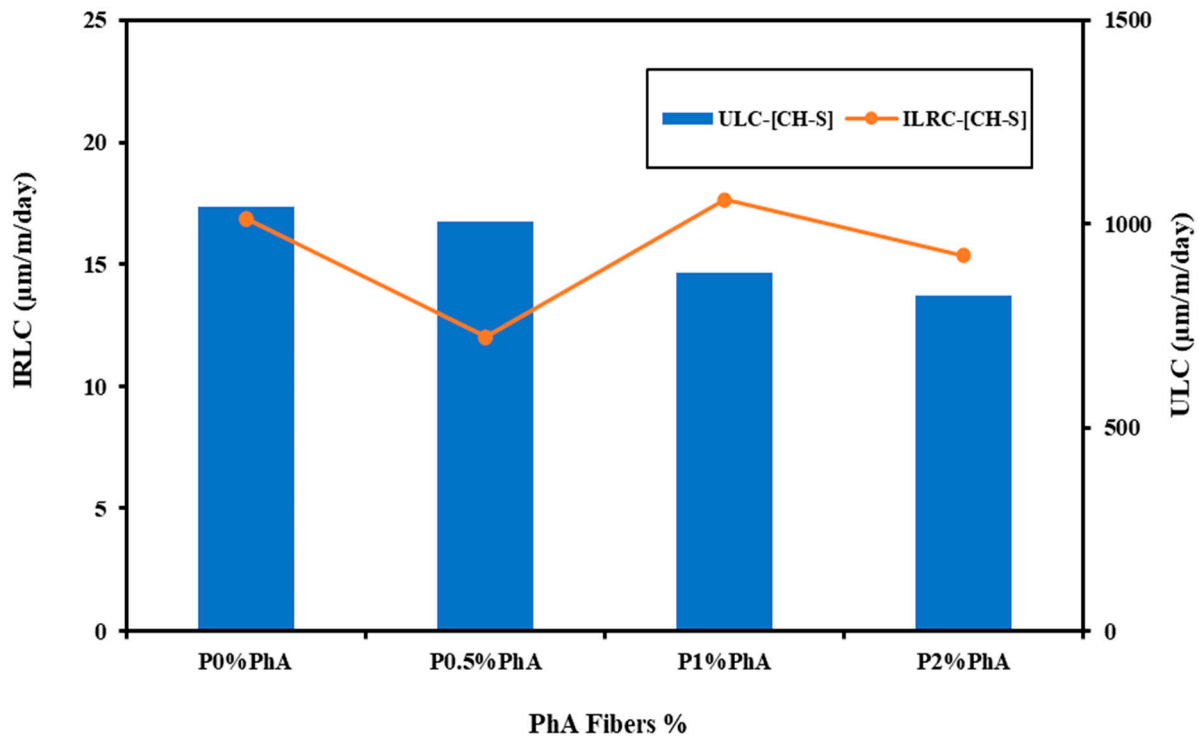


Figure 10. CH-S characteristics for pastes at 45 °C.

3.4.2. Autogenous Shrinkage (AU-S)

Figure 11 illustrates the impact of AU-S at elevated temperatures (45 °C). As depicted, the AU-S seemed to reduce with the addition of PhA fibers. The difference in the AU-S varied depending on the duration. At early stages, the difference in the AU-S was more significant in the presence of fibers. However, at later ages, the difference was reduced. For

example, at 60 days, the AU-S values of the pastes with 0, 0.5, 1, and 2% were -1655.79 , -1563.9 , -1196.04 , and -1095.34 $\mu\text{m}/\text{m}$, respectively. This reduction was 5.5, 27.8, and 33.8% lower compared to the control. However, this effect was reduced to 1.3, 5.3, and 10% at 180 days. These findings indicate the crucial role of PhA fibers in reducing shrinkage. This could be attributed to the pores within the fibers, which may act as reservoirs for water storage and release during the curing stage [44,45].

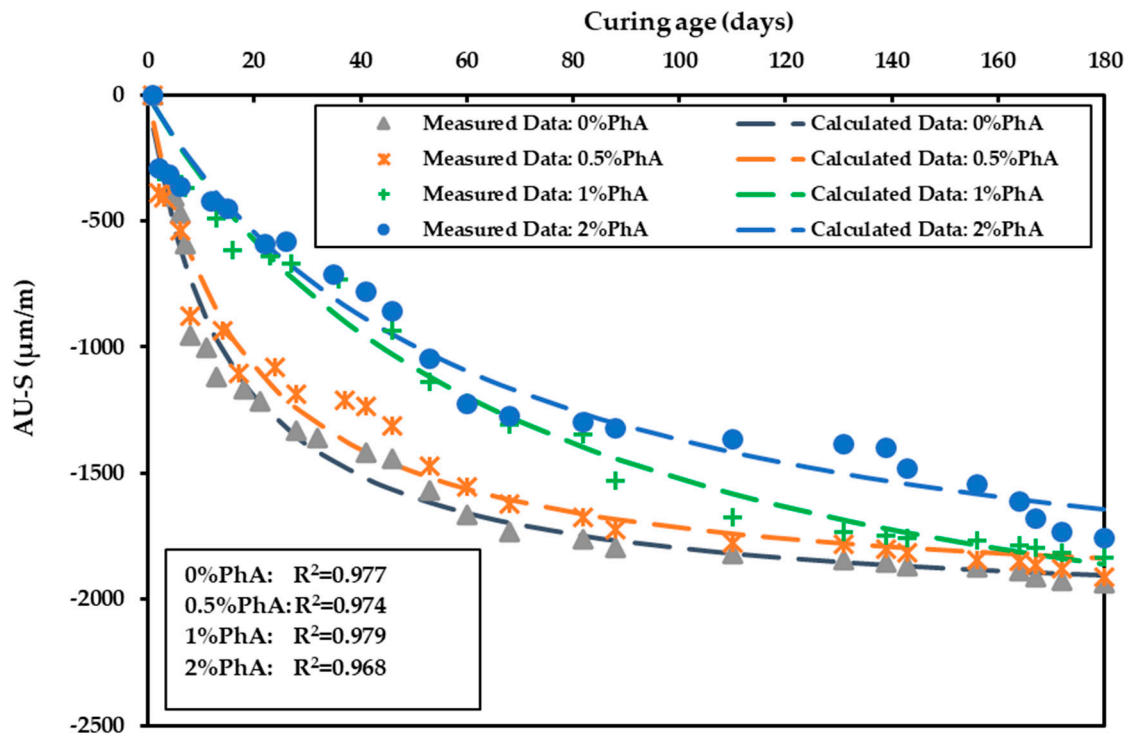


Figure 11. Estimation of AU-S for cement paste specimens at 45 °C.

The experimental data were fitted using the hyperbolic model proposed earlier. The comparison between the calculated and measured AU-S values demonstrates the accuracy of the proposed model, with a high coefficient of determination (R^2) for all the paste mixes ranging from 0.969 to 0.980.

Analyzing how PhA fibers affect the ILRC and ULC of AU-S is very important. As shown in Figure 12, the ILRC exhibited a downward trend in the presence of PhA fibers. For example, the ILRC for the control mix achieved 21.3 $\mu\text{m}/\text{m}/\text{day}$. This value decreased with the addition of 0.5%, 1%, and 2% PhA fibers, reaching values of 19.34, 16.1, and 14.5 $\mu\text{m}/\text{m}/\text{day}$, respectively. This decrease was equivalent to 9.2, 25.5, and 31.9% compared to the control mix. This trend indicates that, during the early stages, PhA fibers absorb moisture effectively, leading to a decrease in the AU-S [46]. Conversely, the ULC showed a decrease with an increase in the PhA fiber content. For example, the ULC for the reference mix attained 2056.3 $\mu\text{m}/\text{m}$ at 180 d. This value dropped with the inclusion of 0.5, 1, and 2% PhA fibers, where values of 2016, 1976, and 1897 $\mu\text{m}/\text{m}$ were recorded, respectively. This was equivalent to a 2%, 4%, and 7.7% decrease with respect to the control mix. The following results suggest that, during the curing stage, PhA fibers begin releasing water from their stored pores, resulting in a reduction in the AU-S as the PhA fiber content increases. These dynamic behaviors underscore the multifaceted influence of PhA fibers on the AU-S process.

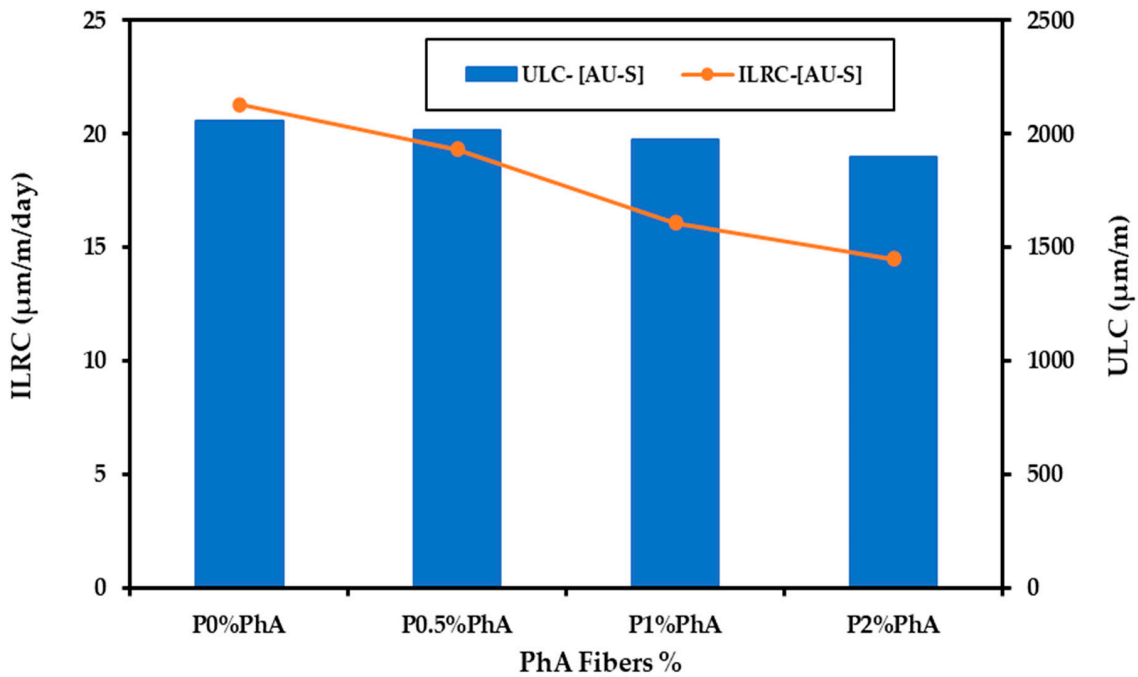


Figure 12. AU-S characteristics for pastes at an elevated temperature.

3.4.3. Drying Shrinkage (DR-S)

Figure 13 displays the DR-S values for pastes containing different proportions of PhA fibers exposed to elevated temperatures (45 °C). Similar to other shrinkage parameters such as CH-S and AU-S, the DR-S results exhibited a consistent trend. The DR-S values dropped as the PhA fiber content increased in the paste mix. For example, at 180 d, the reference mix resulted in 2215 µm/m. This value decreased with the addition of 0.5, 1, and 2% PhA fibers, where it was recorded at values of 2100, 1892, and 1800 µm/m, respectively. This reduction was equivalent to 5.2, 14.6, and 18.7% compared to the reference mix. This may be attributed to the fibers forming bonds with the matrix, which may restrain DR-S [47,48].

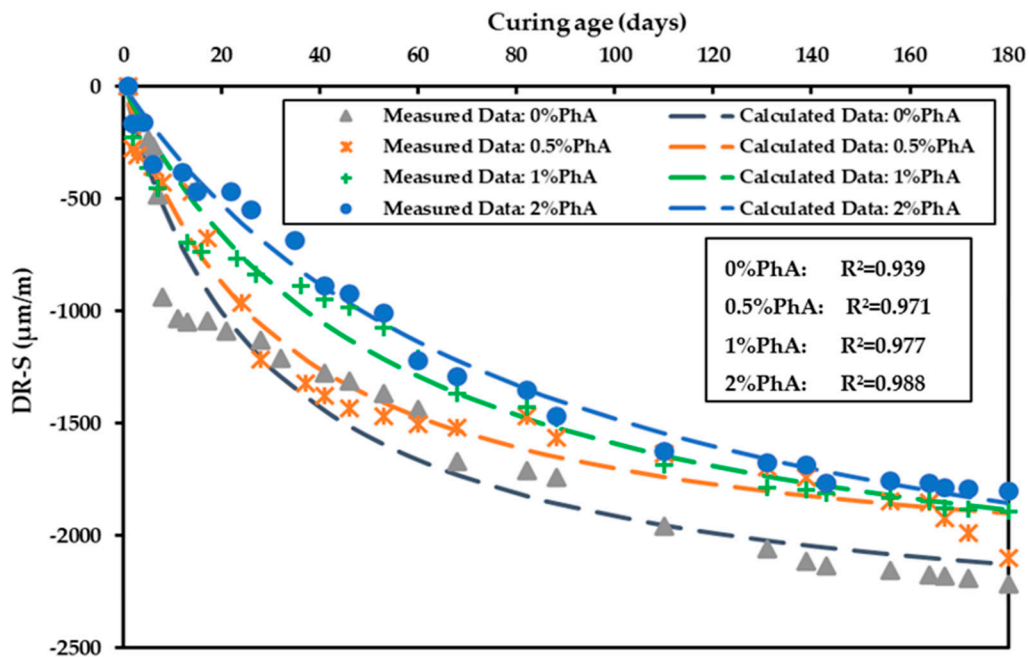


Figure 13. Estimation of DR-S for cement paste specimens at 45 °C.

To determine the DR-S characteristics, the hyperbolic equation was used. The calculated shrinkage data demonstrated an exceptional alignment with the experimental dataset, as the coefficient of determination R^2 achieved values of 0.939, 0.971, 0.977, and 0.988 for 0%, 0.5%, 1%, and 2% PA fibers, respectively.

The ILRC and ULC are presented in Figure 14. As observed, the ILRC exhibited a slight decrease in the presence of 0.5% PhA fibers, followed by a noticeable drop at 1% and 2% PhA fibers. For example, the ILRC for the 0% PhA fiber mix was 30.61 $\mu\text{m}/\text{m}/\text{day}$, whereas the pastes with 0.5, 1, and 2% PhA fibers had ILRC values of 29.45, 23.97, and 22.74, respectively. This corresponded to a decrease of 3.8, 21.7, and 25.7%. This decrease can be attributed to a) the expansion of the matrix during the early stages in the presence of PhA fibers, and b) the loss of cellulose content of the PhA fibers, which became more tightly bonded to each other, thereby restraining the matrix and reducing shrinkage [49].

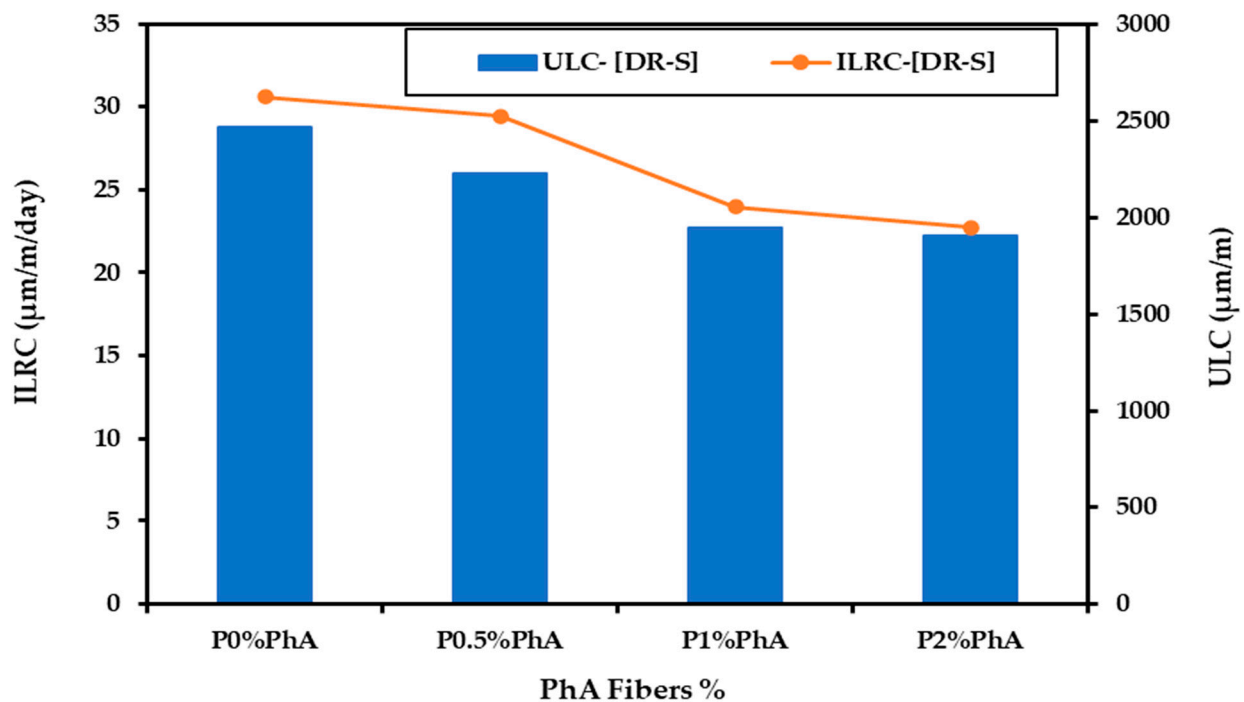


Figure 14. DR-S characteristics for paste at 45 °C.

Additionally, over an extended duration (180 d), DR-S diminished with the addition of PhA fibers. This trend is well reflected in the ULC shrinkage results. For example, the ULC for the reference mix was recorded at 2468 $\mu\text{m}/\text{m}$. This value started to drop with the addition of 0.5, 1, and 2% PhA fibers, where it was recorded at 2225, 1946, and 1906 $\mu\text{m}/\text{m}$, respectively. The decrease ranged from 10 to 23% compared to the reference mix. These results indicate that, in the long term, PhA fibers form a robust bond and contribute to the cohesion of materials within the matrix [35]. This phenomenon is consistent with the findings of the ILRC, where similar percentage decreases were observed with the addition of PhA fibers. This means that the % decrease in the shrinkage was consistent for both parameters, implying that the addition of PhA fibers has a consistent and predictable effect on reducing shrinkage, whether it is in the initial stages (ILRC) or over an extended duration (ULC) [50].

3.4.4. Expansion (EXP)

Figure 15 presents the results of the EXP in pastes under an elevated temperature (45 °C). As noted, the EXP significantly diminished with an addition of PhA fibers of up to 2%. For example, at 180 d, the EXP of the control mix attained a value of 2415 $\mu\text{m}/\text{m}$. This value started to drop with the addition of 0.5, 1, and 2% PhA fibers, where it was

recorded at values of 2376, 2287, and 2190 $\mu\text{m}/\text{m}$, respectively. This is equal to a decrease of 1.6, 5.3, and 9.3%, respectively, compared to the reference mix. This drop is mainly attributed to the application of PhA fibers during mixing, which may restrict the EXP of the matrix [10,24,25].

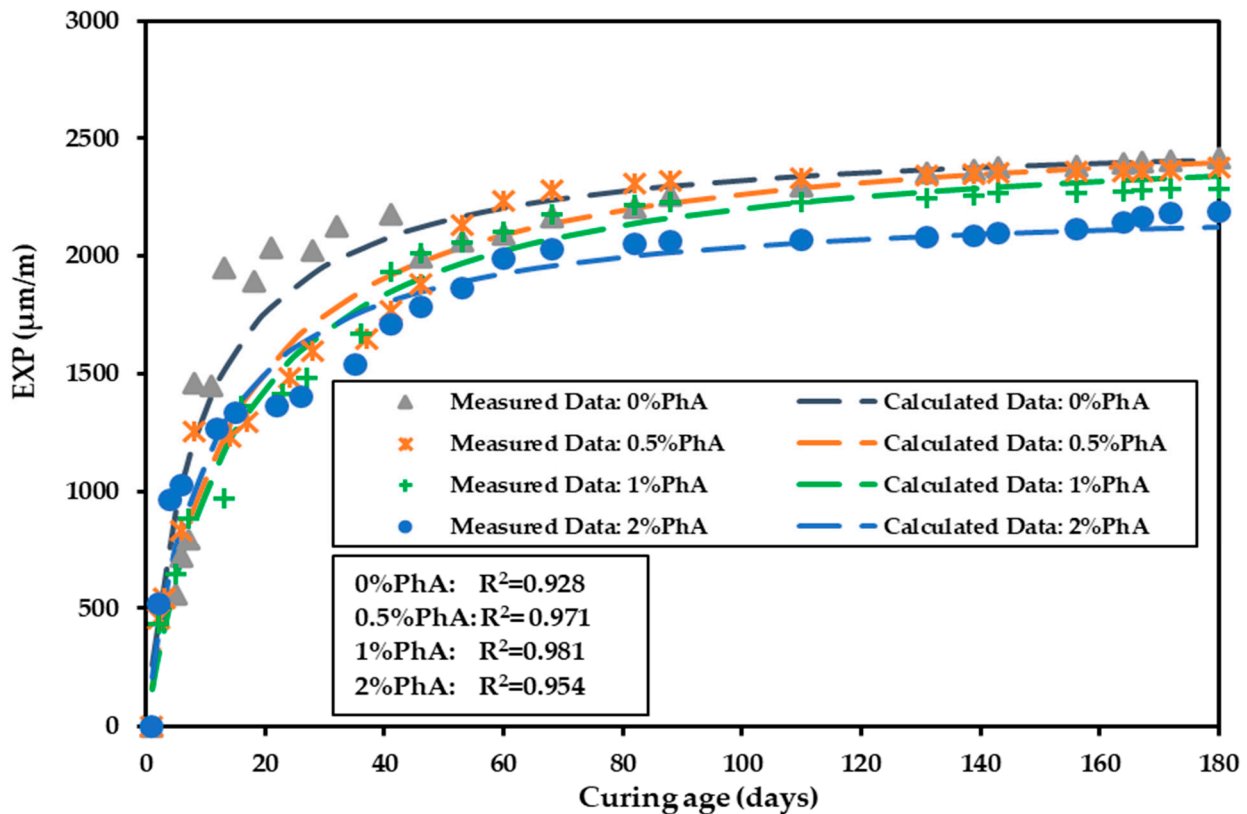


Figure 15. Estimation of EXP for cement paste specimens at 45 °C.

Similar to CH-S, AU-S, and DR-S, the EXP data were fitted using the hyperbolic model. The calculated EXP data shown in Figure 16 showed a remarkable alignment with the experimental EXP data. The notably high coefficient of determination (R^2) underscores the exceptional precision of this model. The R^2 values reached 0.928, 0.970, 0.981, and 0.954 with the addition of 0%, 0.5%, 1%, and 2% PhA fibers, respectively.

The plots for the ILRC and ULC for the EXP characteristics are presented in Figure 16. As depicted, the ILRC decreased as the percentage of PhA fibers increased. For example, the ILRC for the mix with 0% PhA fibers was 259 $\mu\text{m}/\text{m}/\text{day}$. This value began to reduce in the mixes with 0.5%, 1, and 2% PhA fibers and achieved a value of 169, 155, and 108 $\mu\text{m}/\text{m}/\text{day}$, respectively, which was equivalent to 34.75, 40.15, and 58.31%, respectively, compared to the control mix. A similar trend was observed for the ultimate matrix EXP. For example, the ULC for the control mix reached 2526.54 $\mu\text{m}/\text{m}$ at 180 d. Then, the ULC decreased with an increase in the content of PhA fibers and was recorded at 2488, 2437, and 2237 $\mu\text{m}/\text{m}$ for the additions of 0.5, 1, and 2% PhA fibers, which was equivalent to a 1.54, 3.52, and 11.44% decrease, respectively, compared to the reference mix. These outcomes indicate that, during the early stages of curing at an elevated temperature (45 °C \pm 1) and up to a certain percentage addition (2%), the EXP decreases due to the presence of PhA fibers in the matrix [51,52]. PhA fibers exhibit a high water absorption, initially absorbing water and thus augmenting the matrix's EXP. However, with a higher quantity of PhA fibers added, the EXP begins to reduce. This is attributed to the random distribution of PhA fibers, forming a microstructural system that restrains the matrix EXP [24,25,53].

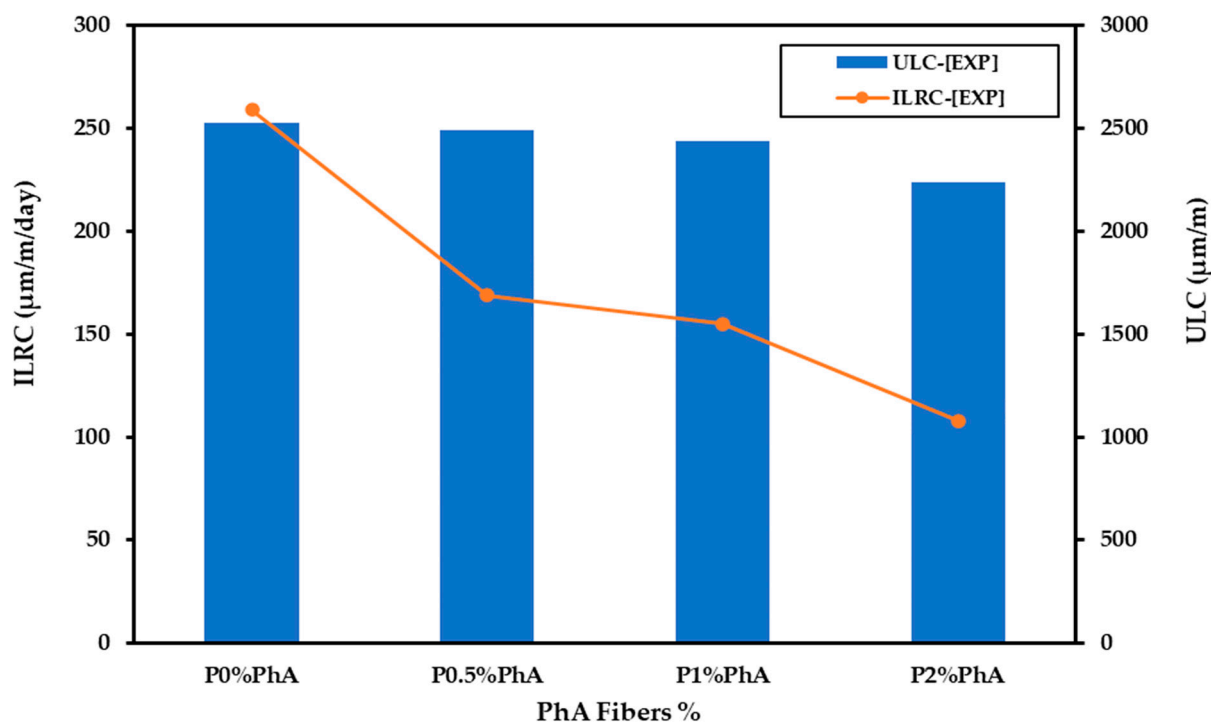


Figure 16. EXP characteristics for pastes at 45 °C.

3.5. Correlations between Shrinkage Parameters

Figures 17–19 provide insights into the correlation between CH-S and various shrinkage parameters, including AU-S and DR-S, as well as EXP. Figure 17 reveals a high correlation between CH-S and DR-S. These types of volume reductions occur through different mechanisms, but display a strong correlation (R^2 ranging between 0.8 and 0.95). CH-S occurs early in the hydration process as cementitious materials react with water, leading to a decrease in volume. In contrast, DR-S occurs later, during the drying and aging of the material after it has hardened [54,55]. The amount of DR-S depends on factors such as the water content, the relative humidity, the temperature, and the pore structure. Despite their distinct mechanisms, both CH-S and DR-S contribute to the overall shrinkage of cementitious materials, collectively known as total shrinkage [56,57]. The magnitude of total shrinkage is of great importance for material durability, as excessive shrinkage can result in cracking and other forms of damage.

A significant correlation was observed in Figure 18 between CH-S and AU-S with a high coefficient of determination, $R^2 > 0.92$. This correlation can be attributed to the various stages that cement pastes undergo during the hydration process. In fact, during the initial setting period, cement pastes lack a strong enough structure to resist bulk deformation [58,59]. Consequently, a volume reduction caused by hydration leads to bulk AU-S, also known as setting shrinkage on the other side, and a negative correlation between CH-S and EXP exists, as shown in Figure 19. This relationship is well established, primarily because there is no shrinkage during water curing, which results in the EXP of the material. In fact, the negative correlation between CH-S and EXP in the presence of PhA fibers results from the ability of the fibers to absorb and release water, providing a barrier against shrinkage while potentially contributing to EXP [60–62]. Additionally, PhA fibers act as reinforcement within the material matrix, limiting shrinkage and redistributing stresses during expansion. The hydration effects and microstructural changes induced by natural fibers further complicate the relationship between shrinkage and EXP [63–65].

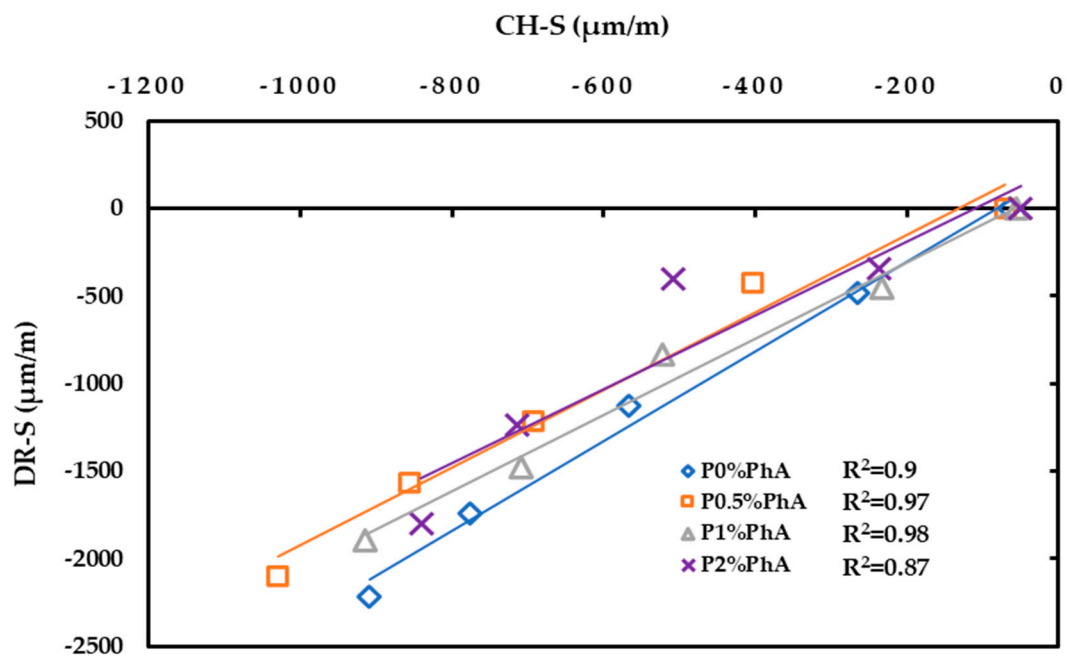


Figure 17. Correlation between CH-S and DR-S for cement paste with PhA fibers at 45 °C.

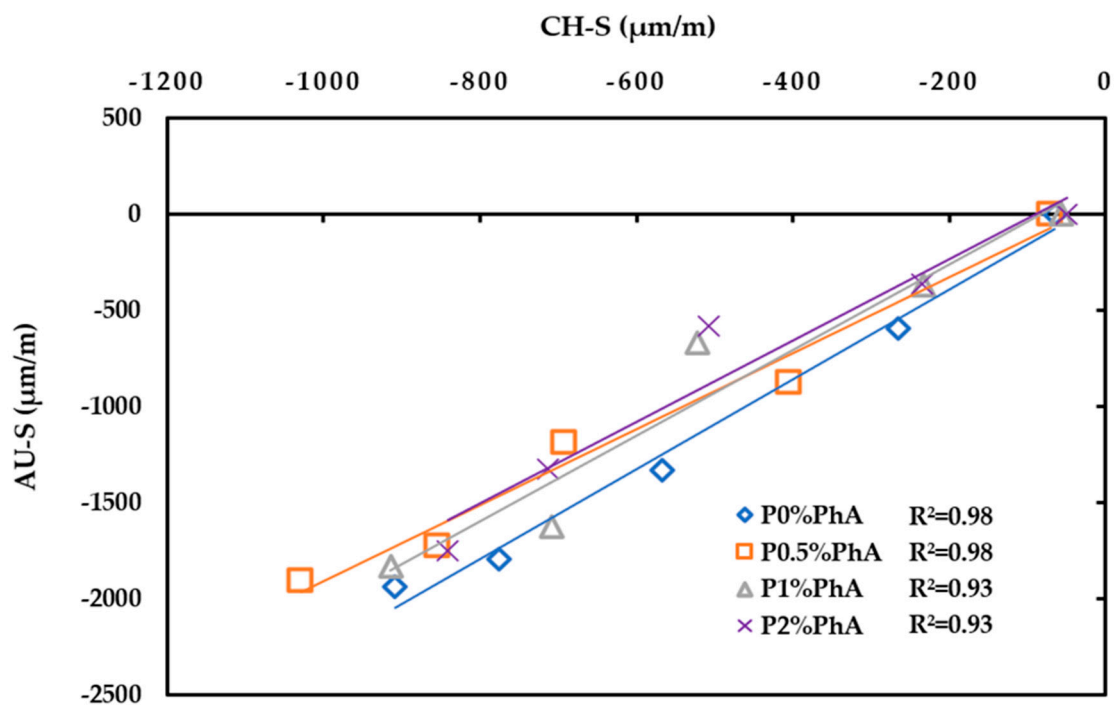


Figure 18. Correlation between CH-S and AU-S for cement paste with PhA fibers at 45 °C.

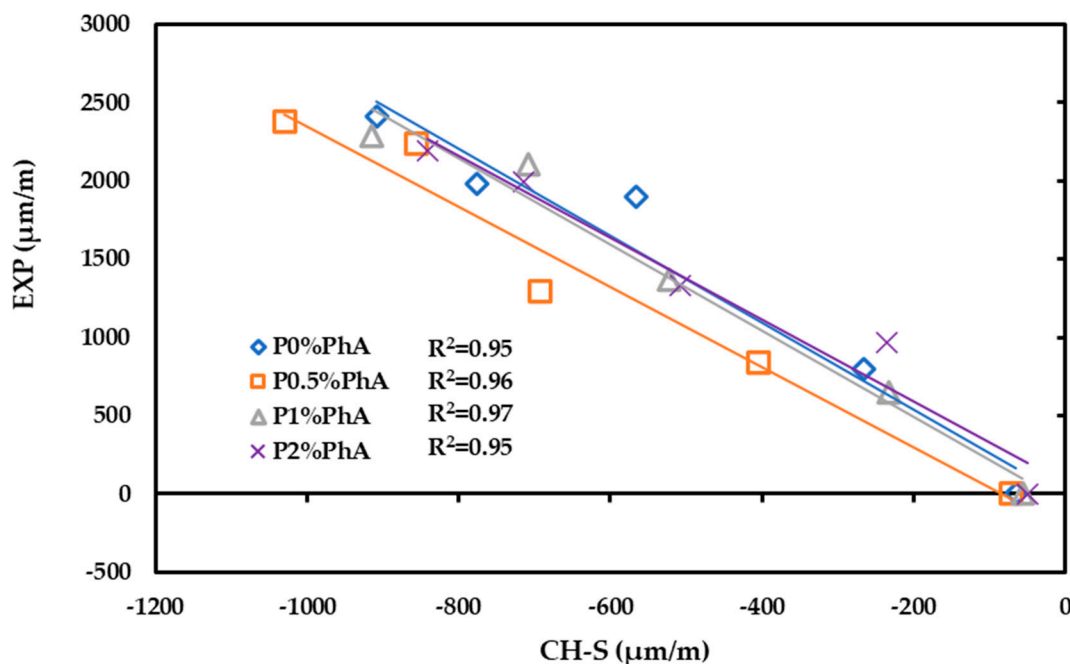


Figure 19. Correlation between CH-S and EXP for cement paste with PhA fibers at 45 °C.

4. Conclusions and Recommendations

This study examined the impact of adding bio-fibers from the Phragmetis-Australis (PhA) plant on selected cement paste properties when subjected to a high temperature. These properties include the compressive strength, flexural strength, chemical shrinkage (CH-S), autogenous shrinkage (AU-S), drying shrinkage (DR-S), and expansion (EXP). Based on the results of this investigation, several points can be made:

- The presence of fibers in the paste resulted in a decrease in the compressive strength. This drop was more noticeable for 2% PhA fibers, where drops of 26.3% and 17.4% were observed at 3 and 180 days, respectively.
- Adding 0.5 and 2% PhA fibers to the mix resulted in a decrease in the flexural strength. At 180 days of curing, this decrease was 3.4 and 22.2% for the paste containing 0.5 and 2% PhA, respectively. However, at 1% PhA fibers, there was a slight increase in the flexural strength, where a 7.5% increase was observed at 180 days.
- Incorporating PhA fibers up to 2% notably reduced the shrinkage and expansion of the paste. In comparison to the control mix, the CH-S, AU-S, DR-S, and EXP decreased by 15.3%, 10%, 18.7%, and 9.3%, respectively, at 180 days.
- The application of the hyperbolic model proved accurate in predicting the length changes over 180 d, with a coefficient of correlation of $R^2 > 0.9$. With an increase in the PhA fiber percentage, there was a consistent reduction in the ultimate length change.
- The high coefficient of determination ($R^2 > 0.8$) showed a positive correlation between the CH-S and the other shrinkage parameters (i.e., AU-S and DR-S). Conversely, there was a negative correlation between CH-S and EXP.
- Understanding the volume stability of a paste can lead to predicting a better behavior for mortar and concrete. Therefore, future research should focus on the volume stability of cementitious systems, such as mortar and concrete, containing PhA fibers. Such research efforts could lead to the development of guidelines for optimizing the use of PhA fibers in various paste applications within the construction industry.

Author Contributions: Conceptualization, H.G.; methodology, R.R. and H.G.; formal analysis, R.R. and H.G.; writing—original draft preparation, H.G. and R.R.; writing—review and editing, J.K. and R.R.; supervision, J.K. and A.E. All authors have read and agreed to the published version of the manuscript.

Funding: This research received no external funding.

Data Availability Statement: Data are contained within the article.

Acknowledgments: The help received from Engineers Nouredine Itani and Zeidoun Zeidan from the faculty of engineering is highly appreciated.

Conflicts of Interest: The authors declare no conflicts of interest.

References

1. Lee, Y.S. Achieving Sustainability in Concrete and Construction: Challenges and Opportunities. *J. Civ. Constr. Eng.* **2022**, *8*, 17–26.
2. Noël, M.; Sanchez, L.; Fathifazl, G. Recent advances in sustainable concrete for structural applications. *Sustain. Constr. Mater. Technol.* **2016**, *4*, 1–11.
3. Kioumars, M.; Plevris, V. Advanced Concrete and Construction Materials for Sustainable Structures. *Sustainability* **2024**, *16*, 1427. [[CrossRef](#)]
4. Hertwich, E.G. Increased carbon footprint of materials production driven by rise in investments. *Nat. Geosci.* **2021**, *14*, 151–155. [[CrossRef](#)]
5. Day, J.W.; Rybczyk, J.M. Global change impacts on the future of coastal systems: Perverse interactions among climate change, ecosystem degradation, energy scarcity, and population. In *Coasts Estuaries*; Elsevier: Amsterdam, The Netherlands, 2019; pp. 621–639. [[CrossRef](#)]
6. Khatib, J.; Ramadan, R.; Ghanem, H.; Elkordi, A. Effect of using limestone fines on the chemical shrinkage of pastes and mortars. *Environ. Sci. Pollut. Res.* **2023**, *30*, 25287–25298. [[CrossRef](#)] [[PubMed](#)]
7. Khatib, J.M.; Ramadan, R.; Ghanem, H.; Elkordi, A.; Sonebi, M. Effect of limestone fines as a partial replacement of cement on the chemical, autogenous, drying shrinkage and expansion of mortars. *Mater. Today Proc.* **2022**, *58*, 1199–1204. [[CrossRef](#)]
8. Khatib, J.M.; Ramadan, R.; Ghanem, H.; Elkordi, A.; Baalbaki, O.; Kirgiz, M. Chemical shrinkage of paste and mortar containing limestone fines. *Mater. Today Proc.* **2022**, *61*, 530–536. [[CrossRef](#)]
9. Ramadan, R.; Ghanem, H.; Khatib, J.; Elkordi, A. Effect of hot weather concreting on the mechanical and durability properties of concrete—a review. *BAU J. Sci. Technol.* **2022**, *4*, 4. [[CrossRef](#)]
10. Khatib, J.; Ramadan, R.; Ghanem, H.; Elkordi, A. Volume Stability of Pastes Containing Limestone Fines. *Buildings* **2021**, *11*, 366. [[CrossRef](#)]
11. Lai, G.; Liu, X.; Li, S.; Xu, Y.; Zheng, Y.; Guan, J.; Gao, R.; Wei, Z.; Wang, Z.; Cui, S. Development of chemical admixtures for green and environmentally friendly concrete: A review. *J. Clean. Prod.* **2023**, *389*, 136116. [[CrossRef](#)]
12. Liu, J.; Yu, C.; Shu, X.; Ran, Q.; Yang, Y. Recent advance of chemical admixtures in concrete. *Cem. Concr. Res.* **2019**, *124*, 105834. [[CrossRef](#)]
13. Ahmad, J.; Majdi, A.; Deifalla, A.F.; Ben Kahla, N.; El-Shorbagy, M.A. Concrete reinforced with sisal fibers (SSF): Overview of mechanical and physical properties. *Crystals* **2022**, *12*, 952. [[CrossRef](#)]
14. Ranjitham, M.; Mohanraj, S.; Ajithpandi, K.; Akileswaran, S.; Sree, S.K. Strength properties of coconut fibre reinforced concrete. In Proceedings of the AIP Conference Proceedings, Tamilnadu, India, 8–9 March 2019; AIP Publishing: Long Island, NY, USA, 2019; Volume 2128.
15. Asim, M.; Uddin, G.M.; Jamshaid, H.; Raza, A.; Hussain, U.; Satti, A.N.; Hayat, N.; Arafat, S.M. Comparative experimental investigation of natural fibers reinforced light weight concrete as thermally efficient building materials. *J. Build. Eng.* **2020**, *31*, 101411. [[CrossRef](#)]
16. Shah, I.; Li, J.; Yang, S.; Zhang, Y.; Anwar, A. Experimental investigation on the mechanical properties of natural fiber reinforced concrete. *J. Renew. Mater.* **2022**, *10*, 1307. [[CrossRef](#)]
17. Abd Khalid, N.H.B.; Yatim, J.M.; Rahman, W.A.W.A. Temperature Effects on Tensile Properties of Kenaf Bast Fiber. In *Empowering Science, Technology and Innovation towards a Better Tomorrow*; UMTAS: Kuala Terengganu, Malaysia, 2011.
18. Hart, A.; Summerscales, J. Effect of time at temperature for natural fibres. *Procedia Eng.* **2017**, *200*, 269–275. [[CrossRef](#)]
19. Placet, V. Characterization of the thermo-mechanical behaviour of Hemp fibres intended for the manufacturing of high performance composites. *Compos. Part A Appl. Sci. Manuf.* **2009**, *40*, 1111–1118. [[CrossRef](#)]
20. Gupta, M.K.; Srivastava, R.K.; Bisaria, H. Potential of jute fibre reinforced polymer composites: A review. *Int. J. Fiber Text. Res.* **2015**, *5*, 30–38.
21. Zhang, D.; Tan, K.H.; Dasari, A.; Weng, Y. Effect of natural fibers on thermal spalling resistance of ultra-high performance concrete. *Cem. Concr. Compos.* **2020**, *109*, 103512. [[CrossRef](#)]
22. Eller, F.; Skálová, H.; Caplan, J.S.; Bhattarai, G.P.; Burger, M.K.; Cronin, J.T.; Guo, W.Y.; Guo, X.; Hazelton, E.L.; Kettering, K.M.; et al. Cosmopolitan species as models for ecophysiological responses to global change: The common reed *Phragmites australis*. *Front. Plant Sci.* **2017**, *8*, 1833. [[CrossRef](#)]

23. Packer, J.G.; Meyerson, L.A.; Skálová, H.; Pyšek, P.; Kueffer, C. Biological flora of the British Isles: *Phragmites australis*. *J. Ecol.* **2017**, *105*, 1123–1162. [\[CrossRef\]](#)
24. Ramadan, R.; Jahami, A.; Khatib, J.; El-Hassan, H.; Elkordi, A. Improving Structural Performance of Reinforced Concrete Beams with *Phragmites Australis* Fiber and Waste Glass Additives. *Appl. Sci.* **2023**, *13*, 4206. [\[CrossRef\]](#)
25. Ramadan, R.; Khatib, J.; Ghorbel, E.; Elkordi, A. Effect of Adding *Phragmites-Australis* Plant on the Chemical Shrinkage and Mechanical Properties of Mortar. In Proceedings of the International Conference on Bio-Based Building Materials, Vienna, Austria, 21–23 June 2023; Springer Nature: Cham, Switzerland, 2023; pp. 573–584.
26. Islam, M.S.; Ahmed, S.J. Influence of jute fiber on concrete properties. *Constr. Build. Mater.* **2018**, *189*, 768–776. [\[CrossRef\]](#)
27. Bheel, N.; Tafsirojjaman, T.; Liu, Y.; Awoyera, P.; Kumar, A.; Keerio, M.A. Experimental study on engineering properties of cement concrete reinforced with nylon and jute fibers. *Buildings* **2021**, *11*, 454. [\[CrossRef\]](#)
28. Jamshaid, H.; Mishra, R.K.; Raza, A.; Hussain, U.; Rahman, M.L.; Nazari, S.; Chandan, V.; Muller, M.; Choteborsky, R. Natural cellulosic fiber reinforced concrete: Influence of fiber type and loading percentage on mechanical and water absorption performance. *Materials* **2022**, *15*, 874. [\[CrossRef\]](#)
29. Ahmad, J.; Arbili, M.M.; Majdi, A.; Althoey, F.; Farouk Deifalla, A.; Rahmawati, C. Performance of concrete reinforced with jute fibers (natural fibers): A review. *J. Eng. Fibers Fabr.* **2022**, *17*, 15589250221121871. [\[CrossRef\]](#)
30. ASTM C 490-04; Standard Practice for Use of Apparatus for the Determination of Length Change of Hardened Cement Paste, Mortar, and Concrete. Annual Book of ASTM Standards 2004, Section 4. vol. 04.02 (Concrete and Aggregates); ASTM: Philadelphia, PA, USA, 2004.
31. ASTM C 1608; Standard Test Method for Chemical Shrinkage of Hydraulic Cement Paste. American Society for Testing and Materials: West Conshohocken, PA, USA, 2007.
32. ASTM C138/C138M-13; Standard Test Method for Density (Unit Weight), Yield, and Air Content (Gravimetric) of Concrete. American Society for Testing and Materials (ASTM) International: West Conshohocken, PA, USA, 2013.
33. ASTM C597; Standard Method for Pulse Velocity Through Concrete. ASTM International: West Conshohocken, PA, USA, 2016.
34. EN 1015-11; Methods of Test for Mortar for Masonry—Part 11: Determination of Flexural and Compressive Strength of Hardened Mortar. British Standards Institution (BSI): London, UK, 2007.
35. Khatib, J.; Ramadan, R.; Ghanem, H.; Elkordi, A. Effect of Adding *Phragmites-Australis* Fiber on the Mechanical Properties and Volume Stability of Mortar. *Fibers* **2024**, *12*, 14. [\[CrossRef\]](#)
36. Ghanem, H.; Ramadan, R.; Khatib, J.; Elkordi, A. A Review on Chemical and Autogenous Shrinkage of Cementitious Systems. *Materials* **2024**, *17*, 283. [\[CrossRef\]](#)
37. Bheel, N.; Sohu, S.; Awoyera, P.; Kumar, A.; Abbasi, S.A.; Olalusi, O.B. Effect of wheat straw ash on fresh and hardened concrete reinforced with jute fiber. *Adv. Civ. Eng.* **2021**, *2021*, 6659125. [\[CrossRef\]](#)
38. Bessadok, A.; Roudesli, S.; Marais, S.; Follain, N.; Lebrun, L. Alfa fibres for unsaturated polyester composites reinforcement: Effects of chemical treatments on mechanical and permeation properties. *Compos. Part A Appl. Sci. Manuf.* **2009**, *40*, 184–195. [\[CrossRef\]](#)
39. Kaplan, G.; Bayraktar, O.Y. The effect of hemp fiber usage on the mechanical and physical properties of cement-based mortars. *Res. Eng. Struct. Mater.* **2021**, *7*, 245–258. [\[CrossRef\]](#)
40. Othuman Mydin, M.A.; Mohd Zamzani, N.; Abdul Ghani, A.N. Influence of elevated temperatures on compressive and flexural strengths of *Cocos nucifera* Linn. fiber strengthened lightweight foamcrete. *Rev. Construcción* **2020**, *19*, 112–126. [\[CrossRef\]](#)
41. Awoyera, P.O.; Odutuga, O.L.; Effiong, J.U.; De Jesus Silvera Sarmiento, A.; Mortazavi, S.J.; Hu, J.W. Development of Fibre-Reinforced Cementitious Mortar with Mineral Wool and Coconut Fibre. *Materials* **2022**, *15*, 4520. [\[CrossRef\]](#)
42. Çavdar, A. A study on the effects of high temperature on mechanical properties of fiber reinforced cementitious composites. *Compos. Part B Eng.* **2012**, *43*, 2452–2463. [\[CrossRef\]](#)
43. Ferreira, S.R.; Silva, L.E.; McCaffrey, Z.; Ballschmiede, C.; Koenders, E. Effect of elevated temperature on sisal fibers degradation and its interface to cement based systems. *Constr. Build. Mater.* **2021**, *272*, 121613. [\[CrossRef\]](#)
44. Zhang, Z.; Scherer, G.W. Measuring chemical shrinkage of ordinary Portland cement pastes with high water-to-cement ratios by adding cellulose nanofibrils. *Cem. Concr. Compos.* **2020**, *111*, 103625. [\[CrossRef\]](#)
45. Ren, G.; Yao, B.; Ren, M.; Gao, X. Utilization of natural sisal fibers to manufacture eco-friendly ultra-high-performance concrete with low autogenous shrinkage. *J. Clean. Prod.* **2022**, *332*, 130105. [\[CrossRef\]](#)
46. Zhutovsky, S.; Kovler, K. Influence of water to cement ratio on the efficiency of internal curing of high-performance concrete. *Constr. Build. Mater.* **2017**, *144*, 311–316. [\[CrossRef\]](#)
47. Khandaker, S.; Akter, D.; Hasan, M.; Saifullah, A.; Marwani, H.M.; Islam, A.; Asiri, A.M.; Rahman, M.M.; Hasan, M.M.; Kuba, T.; et al. From industrial jute fibre spinning wastes to biofibre-reinforced plastics. *Mater. Chem. Phys.* **2024**, *313*, 128586. [\[CrossRef\]](#)
48. Kesikidou, F.; Stefanidou, M. Natural fiber-reinforced mortars. *J. Build. Eng.* **2019**, *25*, 100786. [\[CrossRef\]](#)
49. Miah, M.J.; Li, Y.; Paul, S.C.; Babafemi, A.J.; Jang, J.G. Mechanical strength, shrinkage, and porosity of mortar reinforced with areca nut husk fibers. *Constr. Build. Mater.* **2023**, *363*, 129688. [\[CrossRef\]](#)
50. Nayak, J.R.; Bochen, J.; Gołaszewska, M. Experimental studies on the effect of natural and synthetic fibers on properties of fresh and hardened mortar. *Constr. Build. Mater.* **2022**, *347*, 128550. [\[CrossRef\]](#)

51. Guo, A.; Sun, Z.; Satyavolu, J. Impact of modified kenaf fibers on shrinkage and cracking of cement pastes. *Constr. Build. Mater.* **2020**, *264*, 120230. [[CrossRef](#)]
52. Jaberizadeh, M.M.; Danoglidis, P.A.; Shah, S.P.; Konsta-Gdoutos, M.S. Eco-efficient cementitious composites using waste cellulose fibers: Effects on autogenous shrinkage, strength and energy absorption capacity. *Constr. Build. Mater.* **2023**, *408*, 133504. [[CrossRef](#)]
53. Yıldırım, M.; Özhan, H.B. Durability properties of basalt fiber-reinforced mortars with different mineral admixtures exposed to high temperatures. *Constr. Build. Mater.* **2023**, *400*, 132574. [[CrossRef](#)]
54. Shen, D.; Jiang, J.; Shen, J.; Yao, P.; Jiang, G. Influence of curing temperature on autogenous shrinkage and cracking resistance of high-performance concrete at an early age. *Constr. Build. Mater.* **2016**, *103*, 67–76. [[CrossRef](#)]
55. Liu, H.; Lin, H.; Liu, X.; Wang, J.; Pang, X.; Kong, X. Effects of triethanolamine on autogenous shrinkage and drying shrinkage of cement mortar. *Constr. Build. Mater.* **2021**, *304*, 124620. [[CrossRef](#)]
56. Mermerdaş, K.; Algin, Z.; Ekmen, Ş. Experimental assessment and optimization of mix parameters of fly ash-based lightweight geopolymer mortar with respect to shrinkage and strength. *J. Build. Eng.* **2020**, *31*, 101351. [[CrossRef](#)]
57. Holt, E. Contribution of mixture design to chemical and autogenous shrinkage of concrete at early ages. *Cem. Concr. Res.* **2005**, *35*, 464–472. [[CrossRef](#)]
58. Kucharzyková, B.; Daněk, P.; Kocáb, D.; Misák, P. Experimental analysis on shrinkage and swelling in ordinary concrete. *Adv. Mater. Sci. Eng.* **2017**, *2017*, 3027301. [[CrossRef](#)]
59. Marušić, E.; Štirmer, N. Autogenous shrinkage and expansion related to compressive strength and concrete composition. *J. Adv. Concr. Technol.* **2016**, *14*, 489–501. [[CrossRef](#)]
60. Li, Z.; Guo, T.; Chen, Y.; Yang, W.; Wang, J.; Jin, L. Preparation and properties of pretreated jute fiber cement-based composites. *Ind. Crops Prod.* **2024**, *210*, 118090. [[CrossRef](#)]
61. Song, H.; Liu, J.; He, K.; Ahmad, W.A. comprehensive overview of jute fiber reinforced cementitious composites. *Case Stud. Constr. Mater.* **2021**, *15*, e00724. [[CrossRef](#)]
62. Aluko, O.G.; Yatim, J.M.; Kadir, M.A.A.; Yahya, K. A review of properties of bio-fibrous concrete exposed to elevated temperatures. *Constr. Build. Mater.* **2020**, *260*, 119671. [[CrossRef](#)]
63. Chindapasirt, P.; Boonbamrung, T.; Poolsong, A.; Kroehong, W. Effect of elevated temperature on polypropylene fiber reinforced alkali-activated high calcium fly ash paste. *Case Stud. Constr. Mater.* **2021**, *15*, e00554. [[CrossRef](#)]
64. Fu, Z.; Yao, Y.; Duan, Y.; Wang, B.; Li, X. Failure mechanism of bonding between natural fiber and cement matrix at high temperature. *Constr. Build. Mater.* **2024**, *412*, 134724. [[CrossRef](#)]
65. Santos, S.F.; Teixeira, R.S.; Junior, H.S. Interfacial transition zone between lignocellulosic fiber and matrix in cement-based composites. In *Sustainable and Nonconventional Construction Materials Using Inorganic Bonded Fiber Composites*; Woodhead Publishing: Sawston, UK, 2017; pp. 27–68. [[CrossRef](#)]

Disclaimer/Publisher’s Note: The statements, opinions and data contained in all publications are solely those of the individual author(s) and contributor(s) and not of MDPI and/or the editor(s). MDPI and/or the editor(s) disclaim responsibility for any injury to people or property resulting from any ideas, methods, instructions or products referred to in the content.